Supporting Information

Atmospheric Processes of Aromatic Hydrocarbons in the Presence of Mineral Dust Particles in an Urban Environment

Zechen Yu and Myoseon Jang.*

Department of Environmental Engineering Sciences, Engineering School of Sustainable Infrastructure and Environment, University of Florida, Gainesville, FL, 32611, United States.

*Corresponding author: Myoseon Jang (mjang@ufl.edu)

Number of Figures: 12

Number of Sections: 6

Number of Tables: 2

Section 1: Sample preparation of GDD-BZA and GDD-sodium benzoate

Gobi Desert dust (GDD) particles used in this study were originated from Tsogt-Ovoo soum in the Ömnogövi Province, Mongolia between March and May in 2015. The mass fraction of elements in GDD particles using an energy dispersive spectroscopy (EDS) was reported in the study by Park, et al. [1] Figure S1 illustrates the mass fraction of elements in GDD particles. To study the photocatalytic reaction of organic compounds on dust particles, three different samples: benzoic acid coated GDD (GDD-BZA), sodium benzoate coated GDD and pure sodium benzoate (Sigma Aldrich; ≥99%) were used. GDD-BZA was prepared by putting benzoic acid powder (Sigma Aldrich; ≥99.5%) with dust sample together in a sealed container. Benzoic acid then evaporated and partitioned onto dust particles and reacted with carbonates in the dust. After the reaction was fully completed (verified by measuring the benzoate in dust sample), clean tank air (RH<5%) with flowrate at 0.5 L min^{-1} passed through the sample for 48 hours to remove the excess benzoic acid. The concentration of benzoate in GDD-BZA and sodium benzoate coated GDD is estimated to be 3% of total dry dust mass. The samples for GDD-BZA and pure sodium benzoate were prepared by first nebulize the particles into a 2 m^3 indoor Teflon chamber and then collected using 13 mm diameter Teflon-coated glass fiber filter (Pall Life Science Pallflex TX40HI20-WW). The sodium benzoate coated GDD filter samples were prepared by first collecting raw GDD dust on a Teflon filter and then impregned with sodium benzoate (water solution). Filter samples were dried and weighted by an analytical balance (MX5; Mettler-Toledo Ltd., England).

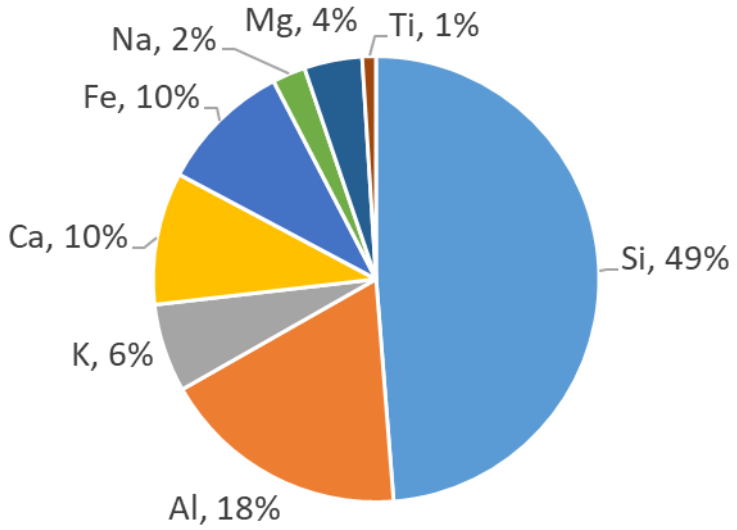

Figure S1. Mass fraction of elements in GDD particles reported by Park, Jang and Yu [1]

Section 2: Outdoor chamber experiments

The outdoor chamber experiments were conducted under sunlight. All the outdoor chamber experiments were operated followed the standard operation procedure for quality control and quality assurance. Before each experiment, the dual chambers were flushed and cleaned by the air purifier system (GC Series, IQ Air Inc.) for more than 48 hours. The background ion concentrations were measured every time before the experiments using a Particle-Into-Liquid Sampler (Applikon, ADISO 2081) combined with Ion Chromatography (Metrohm, 761 Compact IC) (PILS-IC). 1,3,5-Trimethylbenzene (TMB), toluene, and gasoline vapor were injected using a syringe with heating. The gasoline (#93) was purchased from BP. Inc at Gainesville, Florida on May 3, 2018. The composition of gasoline was measured using a gas chromatography-flame ionization detector (GC-FID; HP 5890) and shown in Table S1. Non–reactive CCl_4 (400 ppb) was injected into the dual chamber to determine the chamber dilution factor. NO and NO_2 were injected into the chamber from a tank of 2% NO or NO_2 (Airgas, USA.). Dust particles were introduced into the chamber using a nebulizer (LC STAR, Pari Respiratory Equipment) with the clean tank air. For the experiments in which inorganic seeds were used, a 0.05 mol L^{-1} of ammonium sulfate (AS) solution was atomized using the nebulizer with clean air flow. During the experiments, a gas chromatography-flam ionization detector (HP-5890 GC-FID) was used for monitoring of organic gases. A chemiluminescence NO/NO_x analyzer (Teledyne Model T201) was used for NO_x. And a photometric ozone analyzer (Model 400E, Teledyne, USA) was used for ozone. The particle size distribution was continuously measured by an SMPS (SMPS, TSI 3080, USA) and an Optical Particle Sizer (OPS, TSI 330, USA). The measured particle size distribution was processed using Multi-Instrument Manager Software (MIM2, TSI, USA) and converted to particle size distribution (0-10 μm) in aerodynamic diameter for dust particles. In addition, the rate constant of particle loss to the chamber wall was measured for Gobi Desert Dust (GDD) particles and the ammonium sulfate inorganic seeded aerosol. The concentration of organic carbon was measured by a semi-continuous OC/EC carbon aerosol analyzer (Model 4, Sunset Laboratory Inc., US). The humidity and temperature were measured using a hygrometer (CR1000 Measurement and Control System, Campbell Scientific). The sunlight spectrum and intensity were monitored using a fibro–optical portable spectrometer (EPP2000, Stellar Net Inc., USA) and an ultraviolet radiometer (TUVR, Eppley Laboratory Inc.), respectively. Figure S2 illustrates the consumption of VOCs during chamber experiments (Table 1). Figure S3 shows that time profile of NO_x and ozone. Figure S4

presents the time profiles of temperature and humidity over the course of chamber experiments (also see Table 1). Figure S5 illustrates the time profiles of the concentrations of organic matter produced via the photooxidation of precursors in the presence of NO_x during the experiments (also see Table 1).

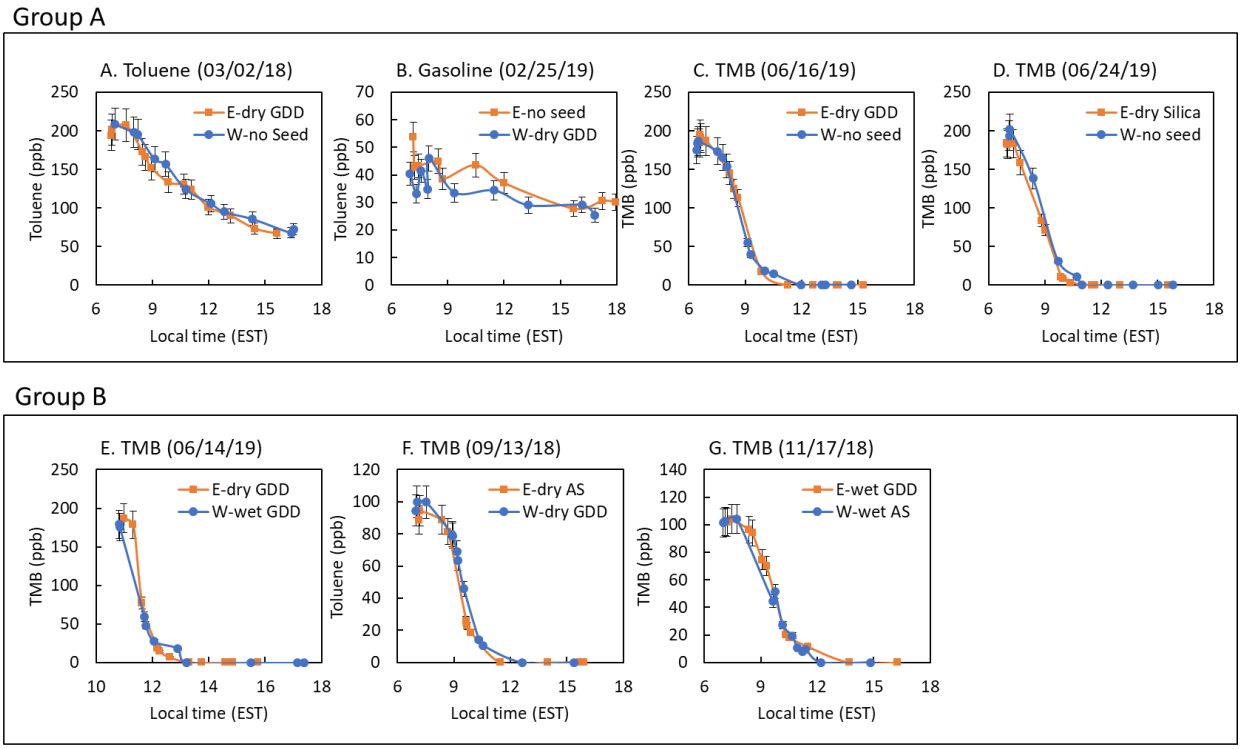

Figure S2. Time profiles of volatile organic compound (VOC) consumption for (A) toluene (03/02/18), (B) gasoline (02/25/19), (C) trimethylbenzene (TMB) (06/16/19), (D) TMB (06/24/19), (E) TMB (06/14/19), (F) TMB (09/13/18), and (G) TMB (11/17/18). For gasoline experiments, toluene concentrations are plotted. The concentration of VOC in the chamber was corrected for the dilution by ambient air. "E" denotes the experiments performed in east chamber and "W" denotes the experiments performed in west chamber. "Group A" is used in Figure 1, 3, and 4 in the main manuscript; "Group B" is used for Figure 6.

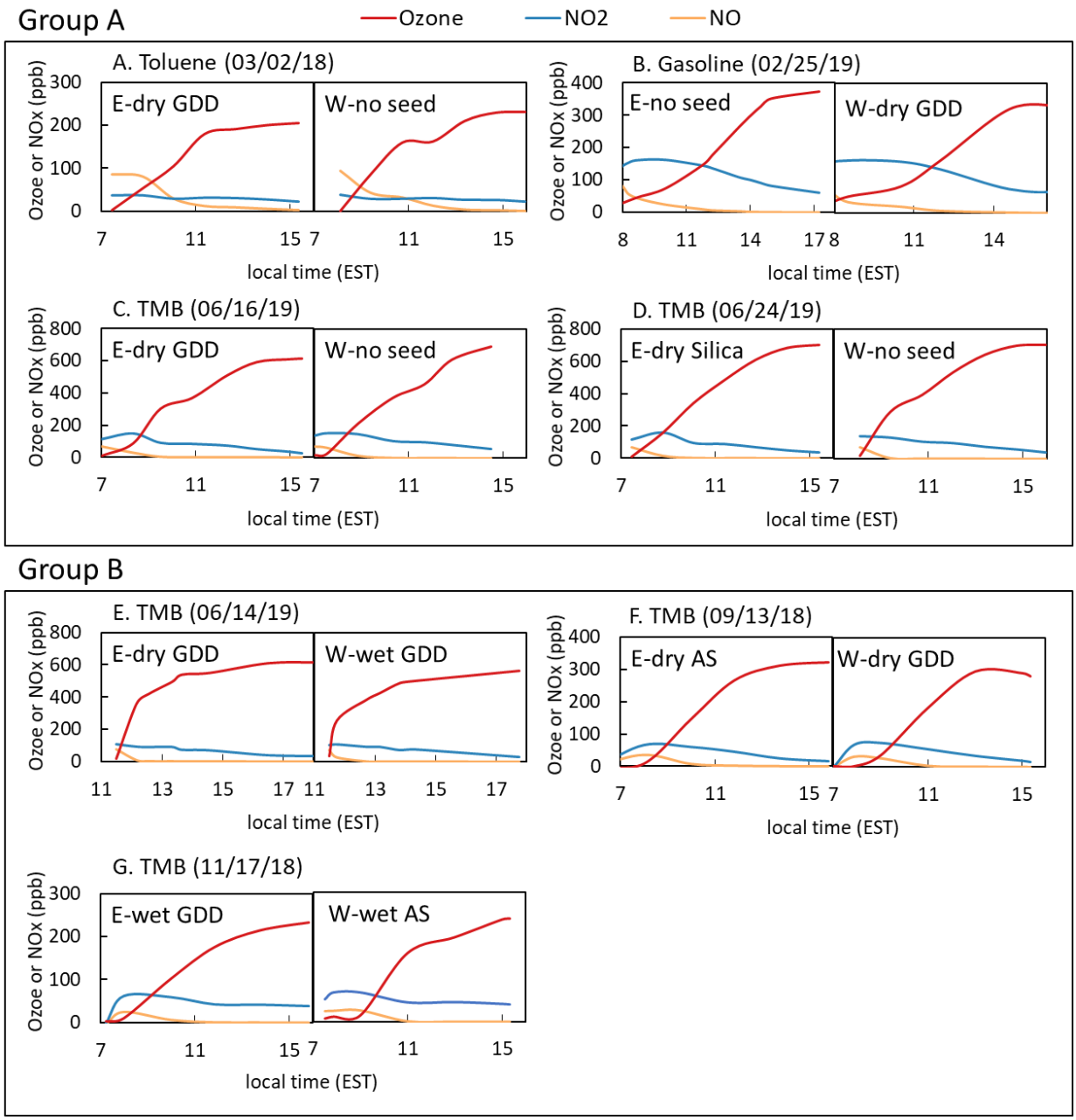

Figure S3. Time profiles of the observed concentrations of ozone, NO and NO_2 for the experiments of (A) toluene (03/02/18), (B) gasoline (02/25/19), (C) trimethylbenzene (TMB) (06/16/19), (D) TMB (06/24/19), (E) TMB (06/14/19), (F) TMB (09/13/18), and (G) TMB (11/17/18). The measurement uncertainties associated with ozone, NO, and NO_2 are ±4.5%, ±6.5% and ±6.5%, respectively. "E" denotes the experiments performed in east chamber and "W" denotes the experiments performed in west chamber. "Group A" is used in Figure 1, 3, and 4 in the main manuscript; "Group B" is used for Figure 6.

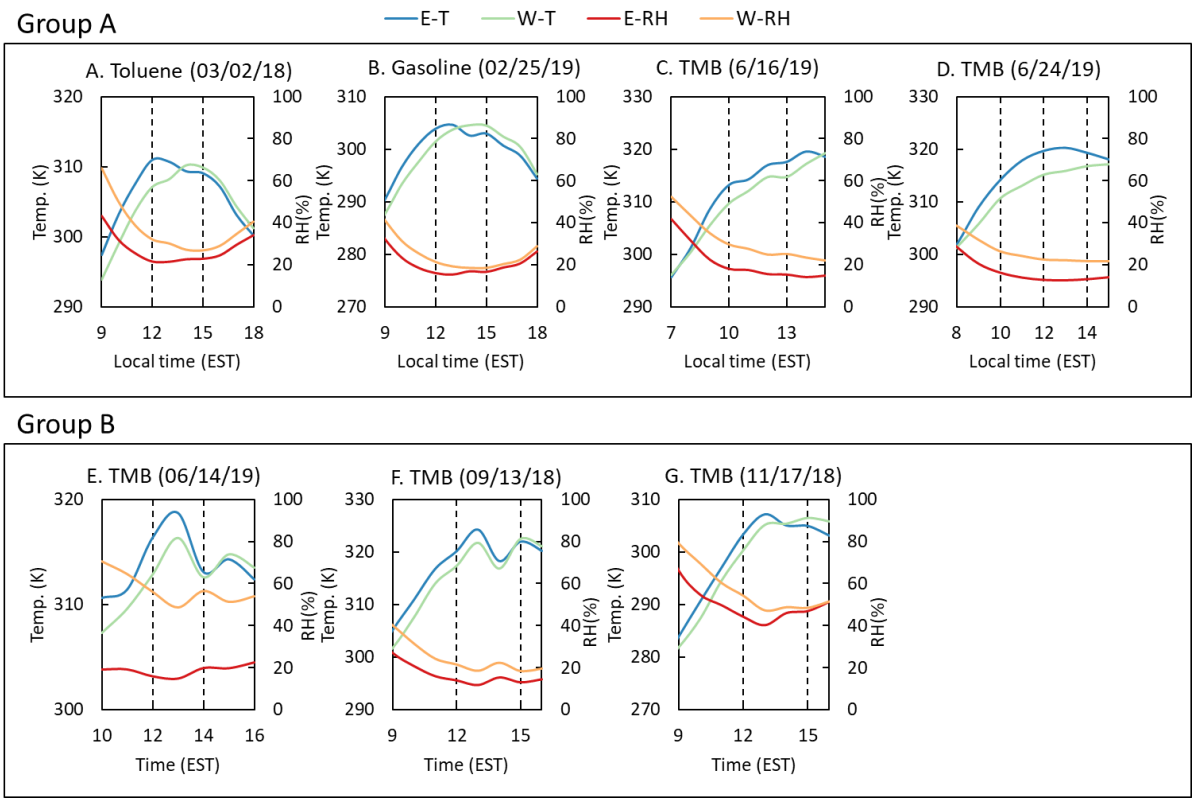

Figure S4. Time profiles of temperature and humidity for (A) toluene (03/02/18), (B) gasoline (02/25/19), (C) trimethylbenzene (TMB) (06/16/19), (D) TMB (06/24/19), (E) TMB (06/14/19), (F) TMB (09/13/18), and (G) TMB (11/17/18). "E" denotes the experiments performed in east chamber and "W" denotes the experiments performed in west chamber. Figures E, F, and G are used for Figure 6 in the main manuscript. "Group A" is used in Figure 1, 3, and 4 in the main manuscript; "Group B" is used for Figure 6.

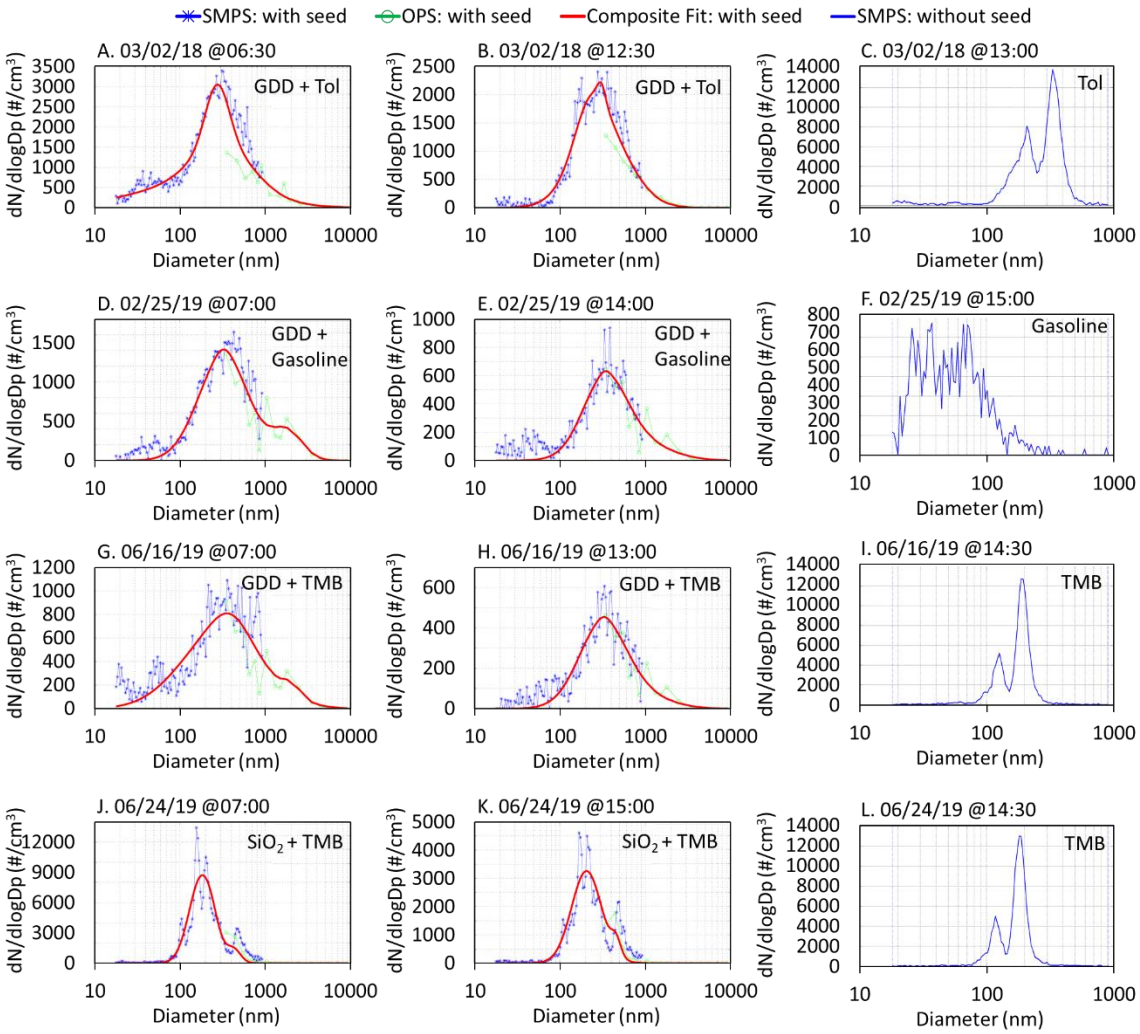

Figure S5. Selected particle size distribution of aerosols for 03/02/2018 (A, B, and C), 02/25/19 (D, E, and F), 06/16/19 (G, H, and I), and 06/24/19 (J, K, and L). The composite particle size distribution was fitted using Multi-Instrument Manager Software (MIM2, TSI, USA).

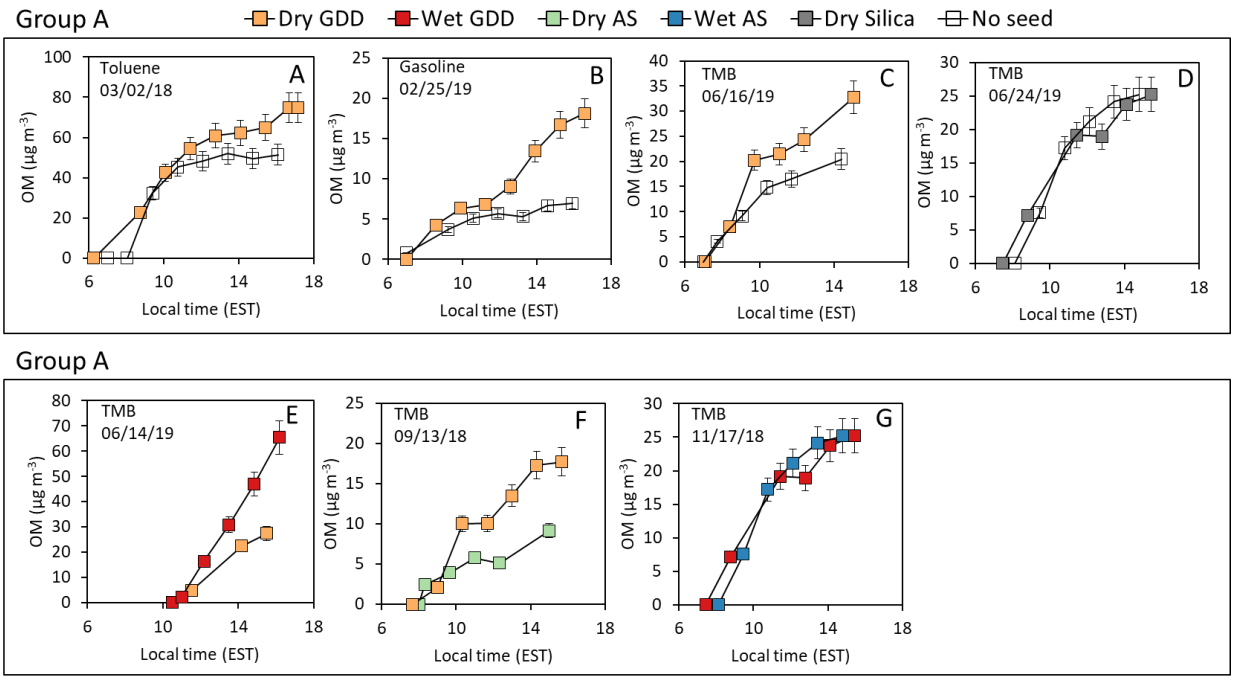

Figure S6. Time profiles of organic matter (OM) concentration over the course of chamber experiments for (A) toluene (03/02/18), (B) gasoline (02/25/19), (C) trimethylbenzene (TMB) (06/16/19), (D) TMB (06/24/19), (E) TMB (06/14/19), (F) TMB (09/13/18), and (G) TMB (11/17/18). The OM concentration was corrected for the particle loss to the chamber wall by the particle deposition rate determined for GDD particles. "Group A" is used in Figure 1, 3, and 4 in the main manuscript; "Group B" is used for Figure 6.

Table S1. Composition of gasoline vapor measured using GC-FID

Chemical species		ppbC per 100 ppbC of gasoline vapor [a]	k_{OH} (cm^3 molecular^{-1} s^{-1})[b]
Alkanes	Neopentane	9.4	
	Iso-Pentane	2.4	
	n-Pentane	0.6	
	Hexane isomers	6.5	
	3-Methylpentane	3.0	
	n-Hexane	2.7	
	2,4-Dimethylpentane	3.0	
	Methylhexanes	4.6	
	2,2,4-Trimethylpentane	10.0	
	Heptane	1.8	
	octanes	8.7	
	Others[c]	~2	
	Total	**54.6**	
Alcohols	Ethanol	9.0	
	Total	**9.0**	
Aromatics	Benzene	1.5	1.22×10^{-12}
	Toluene	13.6	5.63×10^{-12}
	Ethylbenzenes	4.3	7.00×10^{-12}
	m- and p- Xylene	10.5	2.31×10^{-11} and 1.43×10^{-11}
	o-Xylene	4.6	1.36×10^{-11}
	1,3,5-Trimethylbenzene	1.4	5.67×10^{-11}
	1,2,4-Trimethylbenzene	2.1	3.25×10^{-11}
	1,2,3-Trimethylbenzene	0.3	3.27×10^{-11}
	Total	**38.3**	

[a] The composition of gasoline was measured using a GC-FID with a 15m length column (0.25mm I.D. with 0.5 μm film). The errors associated with the measured gasoline composition is ±10% according to the instrumental error of GC-FID.
[b] The reaction rate constant organic compound *i* with OH radicals in gas phase. The values were obtained from the Master Chemical Mechanism (MCM V3.3.1).[2] The values were used to calculate the consumption of aromatic HCs in gasoline experiments and the associated SOA yield.
[c] Due to the detection limits, a small portion of alkanes are not identified (i.e., long chain alkane).

Section 3: Peak assignments in FTIR spectra data

Table S2. The peak assignments of FTIR spectra (Figure 3) for toluene SOA and gasoline SOA in the presence and in the absence of Gobi Desert dust particles.

Functional group	FTIR frequency (cm^{-1})	Reference
O-H st in COH, COOH, or H_2O[a]	2400-3600	Jang and Kamens [3], Li, et al. [4], Jia and Xu [5]
C-H st	2800-3100	Jang and Kamens [3], Li, Jang and Beardsley [4]
C=O st in COOH	1700-1740	Hasan, et al. [6], Xu and Koel [7]
C=C st (conjugated alkene)	1640	Jang and Kamens [3]
C=O st in COO^- or H_2O[a]	1620	Xu and Koel [7], Tang, et al. [8], Ma, et al. [9]
C-O st in COO^-	1420	Tang, Larish, Fang, Gankanda and Grassian [8], Ma, Liu, Liu and He [9]
NO_3^- st	1380	Figure S7-B, Goodman, et al. [10]
Si-O-Si	1040	Gray [11], Figure S7-A

[a] Water is negligible because FTIR spectra were measured under the dry condition by purging with tank air (RH<5%).

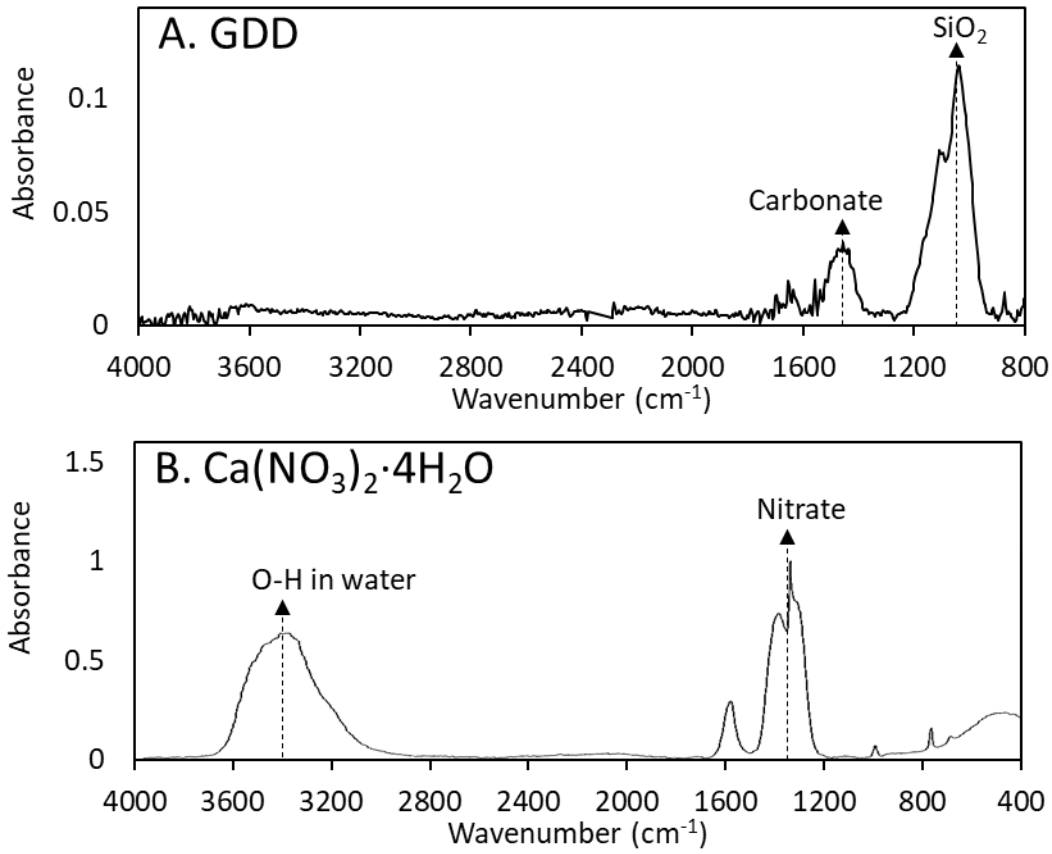

Figure S7. The FTIR spectra of (A) fresh Gobi Desert dust particles measured in this study and (B) calcium nitrate tetrahydrate (Copyright © 1980, 1981-2018 Bio-Rad Laboratories, Inc.). The peaks at 1450 cm^{-1}, and 1040 cm^{-1} in spectrum A represent carbonate and Silica, respectively. The peaks at 3400 cm^{-1} and 1380 cm^{-1} in spectrum B represent H_2O and NO_3^-, respectively.

Section 4: Oxidation and lifetime of organic products on dust particles

The semivolatile organic compounds (SVOCs) partitioned onto dust particles can be oxidized by the OH radicals generated during the photocatalytic activation process of dust particles. The oxidation state of SOA can be characterized by the atomic oxygen-to-carbon (O/C) ratio. In general, O/C is determined using the high-resolution time-of-flight aerosol mass spectrometry to distinguish isomers that differ in elemental compositions [12-14]. Additionally, all constituents in aerosols that are impacted on an ionizer should be evaporated to be detected. However, the evaporation of calcium salts including inorganic anions (i.e., sulfate) and organic carboxylic salts is notorious for the poor evaporation under the typical operational condition (at 600 °C) of the aerosol mass spectrometry. Although the O:C ratio of dust-seeded SOA was not measured with our analytical instrument, a dramatic change in aerosol compositions was observed between toluene SOA and dust-seeded toluene SOA using FTIR data. For example, the FTIR spectrum of toluene SOA clearly showed an OH stretching in carboxylic acids with a long tailing between 3700 and 2100 cm^{-1}. However, this OH stretching in carboxylic acid peaks disappeared in dust-seeded toluene SOA due to the formation of calcium carboxylate salts. The impact of dust particles on the oxidation state of SOA has been reported previously by Liu, et al. [15] that O to C ratio of α-pinene SOA was increased on TiO_2 particles compare to SiO_2 particles under UV light. However, those studies were carried out in the presence of pure metal oxides with alkaline carbonates that are abundant in authentic mineral dust particles.

SOVC that generated via the photooxidation process in gas phase partitioned onto dust particles. The gas-dust partitioning constant ($K_{dust,i}$, m^3 μg^{-1}) of $SVOC_i$ can be described as,[16]

$$K_{dust,i} = \frac{C_{i,dust}}{C_{i,gas} \cdot M_{water}} \quad \text{(S4-1)}$$

where $C_{i,dust}$ (μg m^{-3}) is the concentration of compound $SVOC_i$ in dust phase, $C_{i,gas}$ (μg m^{-3}) is the concentration of compound i in gas phase, and M_{water} (μg m^{-3}) is the total concentration of water content in dust particles. Thus, the total concentration of $SVOC_i$, $C_{i,total}$ (μg m^{-3}), can be written as,

$$C_{i,total} = C_{i,gas} + C_{i,dust}. \quad \text{(S4-2)}$$

The theoretical $K_{dsut,i}$ can be estimated as follows.[16, 17]

$$K_{p,i} = \frac{7.501RT}{10^9 MW_i \gamma_i P_{L,i}} \quad \text{(S4-3)}$$

where T (K) is the temperature, R (8.314 J mol^{-1} K^{-1}) is the ideal gas constant, γ_i is the activity coefficient of SVOC$_i$ in aqueous phase, $P_{L,i}$ is the saturated vapor pressure (mmHg) of SVOC$_i$ and MW_i (g mol^{-1}) is the average molecular weight of an organic medium (water). Dust-phase SVOC can be oxidized by the OH radicals created via photocatalytic processes on dust particles to form either less volatile highly oxygenated multifunctional products (HOM) or more volatile intermediate volatile organic compounds (IVOCs) as follows,

$$\mathrm{SVOC}_i(\mathrm{dust}) +\cdot\ \mathrm{OH}(\mathrm{dust}) \rightarrow \alpha_1\mathrm{HOM}_1 + \cdots + \beta_1\mathrm{IVOC}_1 \ldots + \mathrm{CO}_2 + \mathrm{H}_2\mathrm{O} \quad k_{dust\_OH,i} \qquad \text{(S4-4)}$$

where $k_{dust\_OH,i}$ (cm^3 molecular^{-1} s^{-1}) is the reaction rate constant of SVOC$_i$ with a OH radical on dust particles. Similar, gas-phase SVOC_ican be oxidized by OH radicals as,

$$\mathrm{SVOC}_i(\mathrm{gas}) +\cdot\ \mathrm{OH}(\mathrm{gas}) \rightarrow \mathrm{Product}(\mathrm{gas}) + \mathrm{CO}_2 + H_2O \quad k_{OH,i} \qquad \text{(S4-5)}$$

where $k_{gas\_OH,i}$ (cm^3 molecular^{-1} s^{-1}) is the reaction rate constant of SVOC with an OH radical in gas phase. In general, the characteristic time scale for gas-particle partitioning is very short compared to those for chemical reactions. The degradation rate of organic compound in dust phase can be written as,

$$\frac{\mathrm{d}C_{i,dust}}{dt} = k_{dust\_OH,i} \cdot C_{OH,dust} \cdot C_{i,dust} \qquad \text{(S4-6)}$$

where $C_{OH,dust}$ (molecular cm^{-3}) is the concentration of OH radicals in dust phase. Similarly, the reaction rate of SVOC with OH radicals in gas phase is expressed as,

$$\frac{\mathrm{d}C_{i,gas}}{dt} = k_{gas\_OH,i} \cdot C_{OH,gas} \cdot C_{i,gas} \qquad \text{(S4-7)}$$

where $C_{OH,gas}$ (molecular cm^{-3}) is the concentration of OH radicals in gas phase. By substituting Eq. S4-1 and Eq. S4-2 into Eq. S4-6, we have

$$\frac{\mathrm{d}C_{i,dust}}{dt} = k_{dust\_OH,i} \cdot C_{OH,dust} \cdot \frac{K_{dust,i} \cdot M_{water}}{1+K_{dust,i} \cdot M_{water}} \cdot C_{i,total}\ . \qquad \text{(S4-8)}$$

Thus, the characteristic time (τ_{dust}, s) for the reaction of SVOC with OH radicals on dust particles can be written as,

$$\tau_{dust,OH} = \frac{1+K_{dust,i} \cdot M_{water}}{k_{dust\_OH,i} \cdot C_{OH,dust} \cdot K_{p,i} \cdot M_{water}}\ . \qquad \text{(S4-8)}$$

The characteristic time (τ_{gas_OH}, s) for the reaction of SVOC with OH radicals in gas phase is shown,

$$\tau_{gas,OH} = \frac{1}{k_{gas\_OH,i} C_{OH,gas}}\ . \qquad \text{(S4-9)}$$

$C_{OH,dust}$ and $k_{dust\_OH,i}$ were predicted using the AMAR model[18] at the three RHs (20%, 50% and 80%) at a given sunlight intensity (at 12 pm on 03/02/2018, Exp. 1 in Table 1 and Figure S8). The water content in dust particles was calculated using Eq. 1. For the calculation of $\tau_{gas,OH}$, $k_{gas\_OH,i}$ is set to 10^{-11} cm^3 $molecular^{-1}$ s^{-1} and $C_{OH,gas}$ is set to 10^6 molecular cm^{-3}. For the calculation of τ_{dust_OH}, γ_i is 1 and MW_i is 18 g mol^{-1}. $\tau_{gas,OH}$ and $\tau_{dust,OH}$ were then calculated and applied to Figure S9.

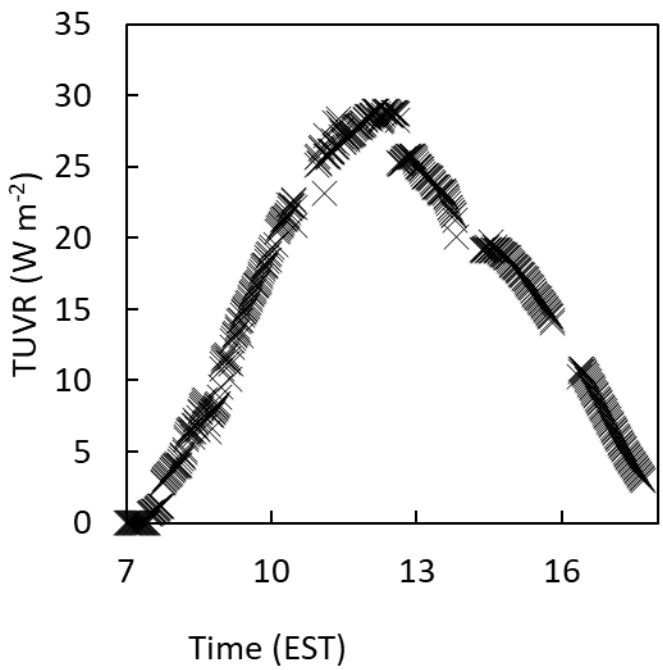

Figure S8. Time profiles of sunlight intensity of experiment on 03/02/2018.

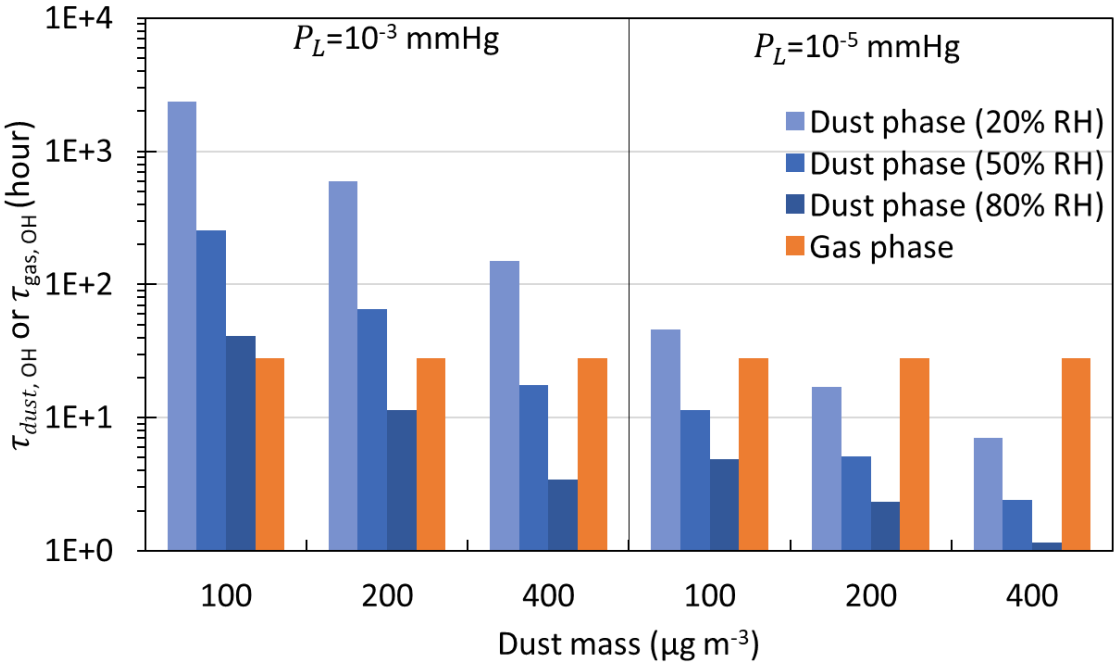

Figure S9. The characteristic time ($\tau_{gas,OH}$, hour) for the reactions of organic species with vapor pressure (P_L, mmHg) of 10^{-4} and 10^{-5} in the gas phase. The characteristic time ($\tau_{dust,OH}$,, hour) for the reactions of organic species with P_L =10^{-4} and 10^{-5} mmHg on the GDD surface under various relative humidity (RH=20%, 50% and 80%). The reaction rate constant of organic species with OH radicals in gas phase is assumed to be 10^{-11} cm^3 molecular^{-1} s^{-1}. The concentration of OH radicals is set to 10^6 molecular cm^{-3} (typical polluted urban environment). The activity coefficient of organic species in aqueous phase is assumed to be 1 and the average molecular weight of an organic medium (water) is set to 18 g mol^{-1}. The TSP is calculated based on Eq. 1 in Section 2.4. the concentration of OH radicals on dust is estimated using the AMAR model based on the sunlight at 12 pm of experiment No. 1 in Table 1.

Section 5: Dust phase water content

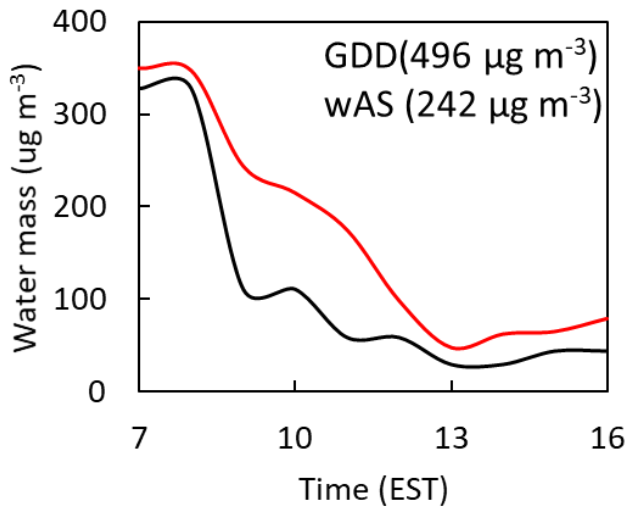

Figure S10. The time profiles of the predicted aerosol water content in the Gobi Desert dust particles (GDD) and ammonium sulfate (AS) particles for the experiment on 11/17/18 (Exp. 13 and 14 in Table 1) using Eq. 1 in Section 2.4. The effect of organic coating on the estimation of water content on GDD particles was not considered. The experimental conditions are shown in Table 1.

Section 6: Concentrations of nitrate and carboxylate in GDD particles over the course of chamber experiments

Figure S11 illustrates the concentration of nitrate measured using PILS-IC over the course of chamber experiments to form TMB SOA (Table 1). Figure S12 shows the depletion of benzoate on GDD particles due to the gaseous nitric acid, which is produced from the photochemical reaction of NO_2 in the UF-APHOR chamber.

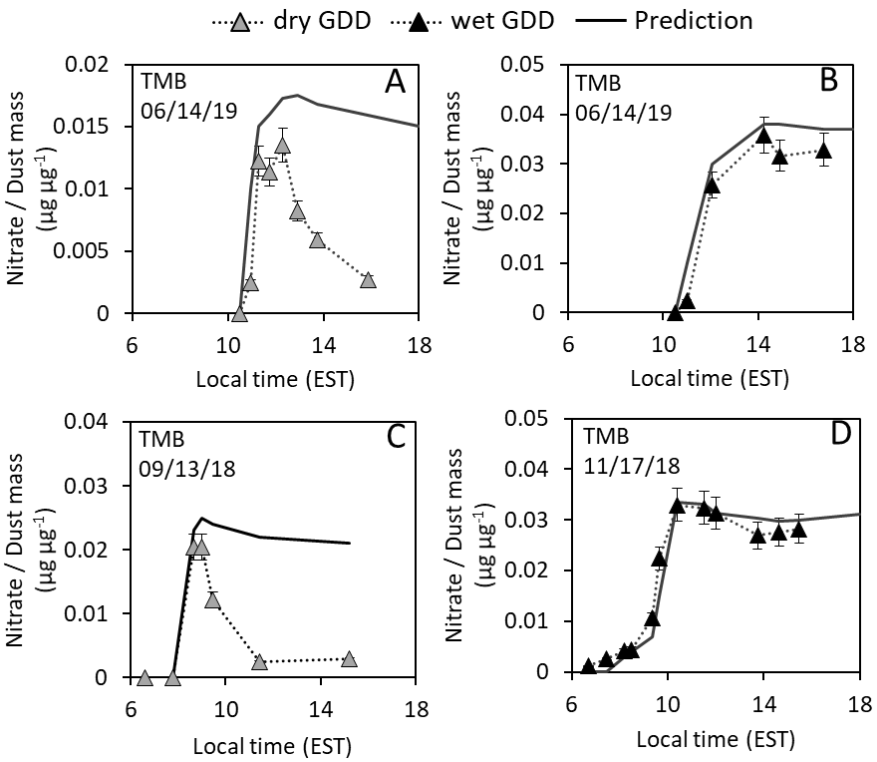

Figure S11. Time profiles of the observed nitrate and predicted nitrate for 1,3,5-trimethylbenzene (TMB) experiments in the presence of GDD for (A) TMB under the dry condition (06/14/19), (B) TMB under the wet condition (06/14/19), (C) TMB under the dry condition (09/13/18), and (D) TMB under the wet condition (11/17/18). The nitrate was also predicted using Atmospheric Mineral Aerosol Reaction (AMAR) Model. [18]

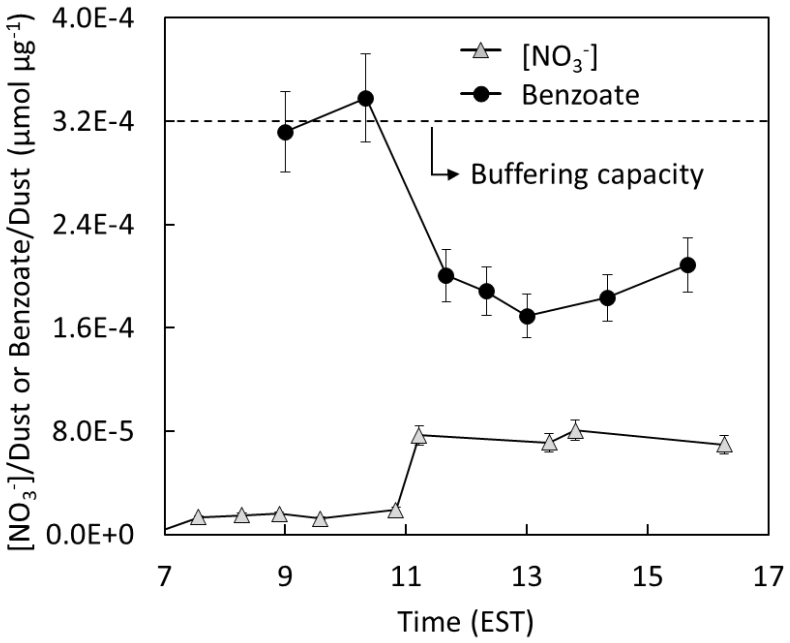

Figure S12. The time profiles of benzoate and nitrate in airborne GDD particles (~400 μg m^{-3}) in the presence of NO_x (130 ppb). The buffering capacity (3.2×10^{-4} μmol μg^{-1}) of GDD particles is reported in the previous study by Yu and Jang [18]. Prior to the chamber experiments, the GDD particles were saturated with benzoic acid as described in Section S1. The experiment was performed using an outdoor chamber under sunlight on 10/13/2018. The benzoate was measured using an organic carbon/elemental carbon (OC/EC) aerosol analyzer and the nitrate was measured using a Particle-Into-Liquid Sampler combined with Ion Chromatography (PILS-IC).

Reference

1. Park, J.; Jang, M.; Yu, Z., Heterogeneous Photo-oxidation of SO_2 in the Presence of Two Different Mineral Dust Particles: Gobi and Arizona Dust. *Environ Sci Technol* **2017,** *51*, (17), 9605-9613.
2. Saunders, S. M.; Jenkin, M. E.; Derwent, R. G.; Pilling, M. J., Protocol for the development of the Master Chemical Mechanism, MCM v3 (Part A): tropospheric degradation of non-aromatic volatile organic compounds. *Atmos Chem Phys* **2003,** *3*, 161-180.
3. Jang, M.; Kamens, R. M., Characterization of secondary aerosol from the photooxidation of toluene in the presence of NO_x and 1-propene. *Environ Sci Technol* **2001,** *35*, (18), 3626-3639.
4. Li, J.; Jang, M.; Beardsley, R. L., Dialkylsulfate formation in sulfuric acid-seeded secondary organic aerosol produced using an outdoor chamber under natural sunlight. *Environ Chem* **2015,** *13*, 690-601.
5. Jia, L.; Xu, Y., Different roles of water in secondary organic aerosol formation from toluene and isoprene. *Atmos. Chem. Phys.* **2018,** *18*, (11), 8137-8154.
6. Hasan, M.; Zaki, M.; Pasupulety, L., Oxide-catalyzed conversion of acetic acid into acetone: an FTIR spectroscopic investigation. *Applied Catalysis A: General* **2003,** *243*, (1), 81-92.
7. Xu, C.; Koel, B. E., Adsorption and reaction of CH_3COOH and CD_3COOD on the MgO (100) surface: A Fourier transform infrared and temperature programmed desorption study. *The Journal of chemical physics* **1995,** *102*, (20), 8158-8166.
8. Tang, M. J.; Larish, W. A.; Fang, Y.; Gankanda, A.; Grassian, V. H., Heterogeneous Reactions of Acetic Acid with Oxide Surfaces: Effects of Mineralogy and Relative Humidity. *J Phys Chem A* **2016,** *120*, (28), 5609-5616.
9. Ma, Q. X.; Liu, Y. C.; Liu, C.; He, H., Heterogeneous reaction of acetic acid on MgO, alpha-Al2O3, and CaCO3 and the effect on the hygroscopic behaviour of these particles. *Phys Chem Chem Phys* **2012,** *14*, (23), 8403-8409.
10. Goodman, A. L.; Bernard, E. T.; Grassian, V. H., Spectroscopic study of nitric acid and water adsorption on oxide particles: Enhanced nitric acid uptake kinetics in the presence of adsorbed water. *J Phys Chem A* **2001,** *105*, (26), 6443-6457.
11. Gray, D. E., *American institute of physics handbook*. American Journal of Physics: 1964; Vol. 32.
12. Aiken, A. C.; Decarlo, P. F.; Kroll, J. H.; Worsnop, D. R.; Huffman, J. A.; Docherty, K. S.; Ulbrich, I. M.; Mohr, C.; Kimmel, J. R.; Sueper, D.; Sun, Y.; Zhang, Q.; Trimborn, A.; Northway, M.; Ziemann, P. J.; Canagaratna, M. R.; Onasch, T. B.; Alfarra, M. R.; Prevot, A. S. H.; Dommen, J.; Duplissy, J.; Metzger, A.; Baltensperger, U.; Jimenez, J. L., O/C and OM/OC Ratios of Primary, Secondary, and Ambient Organic Aerosols with High-resolution Time-of-flight Aerosol Mass Spectrometry. *Environ Sci Technol* **2008,** *42*, (12), 4478-4485.
13. Chhabra, P. S.; Flagan, R. C.; Seinfeld, J. H., Elemental Analysis of Chamber Organic Aerosol using an Aerodyne High-resolution Aerosol Mass Spectrometer. *Atmos Chem Phys* **2010,** *10*, (9), 4111-4131.
14. Canagaratna, M. R.; Jimenez, J. L.; Kroll, J. H.; Chen, Q.; Kessler, S. H.; Massoli, P.; Hildebrandt Ruiz, L.; Fortner, E.; Williams, L. R.; Wilson, K. R.; Surratt, J. D.; Donahue, N. M.; Jayne, J. T.; Worsnop, D. R., Elemental Ratio Measurements of Organic Compounds using Aerosol Mass Spectrometry: Characterization, Improved Calibration, and Implications. *Atmos Chem Phys* **2015,** *15*, (1), 253-272.

15. Liu, Q.; Liggio, J.; Breznan, D.; Thomson, E. M.; Kumarathasan, P.; Vincent, R.; Li, K.; Li, S. M., Oxidative and Toxicological Evolution of Engineered Nanoparticles with Atmospherically Relevant Coatings. *Environ Sci Technol* **2019,** *53*, (6), 3058-3066.
16. Pankow, J. F., An Absorption-Model of Gas-Particle Partitioning of Organic-Compounds in the Atmosphere. *Atmos Environ* **1994,** *28*, (2), 185-188.
17. Odum, J. R.; Jungkamp, T. P. W.; Griffin, R. J.; Flagan, R. C.; Seinfeld, J. H., The atmospheric aerosol-forming potential of whole gasoline vapor. *Science* **1997,** *276*, (5309), 96-99.
18. Yu, Z. C.; Jang, M., Simulation of Heterogeneous Photooxidation of SO_2 and NO_x in the Presence of Gobi Desert Dust Particles Under Ambient Sunlight. *Atmos Chem Phys* **2018,** *18*, (19), 14609-14622.